RESEARCH ARTICLE

DOI: 10.34256/famr2011

Frontiers in Advanced Materials Research

Charge density studies of energetic material: RDX

A. David Stephen [a], S.N. Asthana [b], Rajesh. B. Pawar [b] and P. Kumuradhas [c,*]

[a] Department of Physics, Hindusthan Institute of Technology, Coimbatore 641032, India.

[b] High Energy Material Research Laboratory, DRDO, Sutarwadi, Pune-411 021, India.

[c] Department of Physics, Periyar University, Salem-636 011, India.

* Corresponding Author: kumaradhas@yahoo.com

Received : 5th January 2020, Accepted : 27th January 2020

Abstract: Experimental charge density study has been carried out for Cyclotrimethylene-trinitramine (space group Pbca), an explosive material from a low temperature X-ray diffraction experiment. The electron density was modeled using the Hansen-Coppens multipole model and refined to R=0.032 for 6226 unique observed reflections. The electron density, laplacian and electrostatic potential distributions are reported and discussed, especially, the properties of the bond (3,-1) critical points, which are thought to play a key role in the decomposition of the molecule. From the bond topological analysis of all the bonds, it is observed that the N–N bond is the weakest. The dominating nature of the oxygen atoms was clearly well understood from isosurface electrostatic potential of isolated and symmetrically sitting molecules in the crystal.

Keywords: RDX, Isosurface, Crystal.

1.0 Introduction

Explosives, the energetic material, that was unstable either chemically or energetically and upon initiation, it produces a sudden expansion accompanied by the production of heat and large changes in pressure [1]. From the time of discovery of gun powder [2-4] to modern day explosives, the energetic materials has been of great practical importance. Their contributions in mining, road building and in missile propulsion system were accounted as its significant peaceful uses. Since, the performance of the explosives completely resides on the structural modeling including stable molecular confirmation, inter-intra molecular interactions and thermal vibrational parameters, it is important to understand various electronic and chemical properties at the molecular level [5]. As the conventional single crystal structure determination fails to interpret the chemical bonding nature of the molecules at electronic level, an extensive high resolution diffraction data was required to explicit the charge density distribution in the bonding

region of the molecules. The series of charge density studies on propellants and explosives eg. 5-nitro-2,4-dihyro-3H-1,2,4-triazol-3-one (NTO) [6], two biguanidinium dinitramides [7], pentaerythritol tetranitrate [8], 1,3,4-trinitro-7,8-diazapentalene [9], 3,5,9,11-tetraacetyl-14-oxo-1,3,5,7,9,11-hexaazapenta-cyclo-[5.5.3.02,6.04,10.08,12] pentadecane (CL-20) [10], 1,1-diamino-2,2-dinitro ethylene (FOX-7) [10], were carried out and in these studies, the insights of electron density distribution of these molecules were summarized using high resolution experimental diffraction data. As sustain of this series, in this work, we investigate the energetic material RDX (Cyclotrimethylene-trinitramine) from X-ray diffraction experiment. The conventional methods of structural studies on RDX were carried and structure was first determined by C.S. Choi *et al* [11], reported the geometry of the molecule at room temperature. Here, we do the experimental electron density investigation based on high resolution X-ray diffraction data obtained at low temperature. Using Hansen-Coppens formalism [12], the data were evaluated with a multipole refinement, in which individual atomic densities are described in terms of spherical core and valence densities together with an expression of atom-centered spherical harmonic function.

$$\rho_{atom}(r) = P_c\rho_c(r) + P_v\kappa^3\rho_v(\kappa r) + \sum_{l=0}^{l_{max}} \kappa'^3 R_l(\kappa' r) \sum_{m=0}^{l} P_{lm\pm} Y_{lm\pm}(\theta, \phi)$$

where ρ_c and ρ_v are the spherical core and valence densities, respectively, and the summation in the third term accounts for the valence deformation. P_v is the valance population parameter, which gives the estimate of the net atomic charge. $R_{nl} = r^{nl}\exp(\zeta r)$ is a radial Slater-type function and the coefficients κ and κ' describe the contraction-expansion for the spherical and multipolar valence densities respectively. P_{lm} is the multipole populations and $Y_{lm\pm}$ are the real spherical harmonics of order *l*. Hence the charge density is the exposing tool of the molecular structure at the electronic level, using theory of atoms in molecules [13], which allows extracting the topology of electron density and electrostatic properties of the molecules.

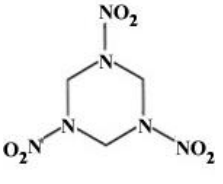

Figure 1. Hexahydro-1,3,5-trinitro-1,3,5-triazine

2.0 Experimental section

RDX was obtained from Defense Research and Development Organization (India). The ground material was crystallized with acetone, by slow evaporation technique at room temperature. From this, nicely shaped and highly transparent crystals of regular size and without any visible growth defects were obtained. A high quality single crystal of dimension 0.4 x 0.4 x

0.4 mm, possessing good morphology was selected for high resolution X-ray intensity data collection. The data collections were carried out using Bruker-Nonius Kappa CCD Area detector system [14]. As a feasible study for charge density analysis, a room temperature data has been collected priory at an X-ray wavelength of 0.71073 Å. For charge density, the sample was cooled to 110 K using stream of cold nitrogen gas. A whole set of X-ray intensity data has been collected up to the resolution $(\sin\theta/\lambda)_{max}$ = 1.2 $Å^{-1}$, of which only the data resolution range of 1.08 $Å^{-1}$, with maximum 2θ value 111.0° for the scan width 0.3°, were taken for crystal structure determination and electron density analysis. All these raw data sets were reduced for Lorentz and Polarization correction using SAINT program [15].

3.0 Spherical and Aspherical model refinement

The structure was solved by Direct methods using SHELXS97 [16] and refined by means of full-matrix least squares procedure using SHELXL97 [17]. All the H-atoms were located using difference fourier map, and these parameters were refined isotropically. The Multipole model charge density refinement was performed with XDLSM routine incorporated to XD [18] program suite. The multipole refinement was carried out on $|F^2|$ using only reflections with $I > 3\sigma(I)$. As a first step, the scale factor is refined using the whole data set and keeping the scale factor fixed, the positional and anisotropic displacement parameters for the non-H atoms were refined using high angle data ($\sin\theta/\lambda > 0.8$ $Å^{-1}$). At this point, all H atom positions were adjusted to neutron distance values [19] [C–H: 1.092 Å]. Since the molecule consists of the same functional groups with identical local chemical environments, the chemical constraints were used extensively in the multipole refinement. The multipole populations of all oxygen atoms of nitrate groups were constrained to O1, those of nitrogen atoms of same to N4, those of N2 and N3 to N1, those of C2, and C3 to C1 and those of all hydrogen atoms to H1. The monopole population, κ, multipole populations and scale were refined with the constraints. At this point, the κ values for H atoms were fixed to theoretical values [20] at 1.2. The charge neutrality was applied throught the refinement. The whole process was repeated until convergence. Using the same chemical constraints, the monopole populations with κ were refined together, followed by the multipole populations, followed by the positional and displacement parameters, followed by the scale factor alone. At this point, reported κ' values [20] were fixed for the all non-H atoms and then refined in the subsequent cycles. In the final refinement the group of parameters P_v, κ, κ', s and P_{lm}, x, y, z respectively were refined separately until all the parameters were converge. The final residual values of multipole refinements details were given in Table 1. Figure 2 presents the residual map after the multipole refinement in the molecular plane, confirms the correctness of the modeling. The total electron density $\rho_{bcp}(r)$, Laplacian $\nabla^2\rho_{bcp}(r)$, the bond, ellipticity ε at the bond critical points (BCP's) and eigen values (λ_1, λ_2, λ_3) were calculated by using XDPROP routine. The deformation density Δρ and Laplacian electron density $\nabla^2\rho$ maps were plotted using XDGRAPH routine incorporated to XD program suite.

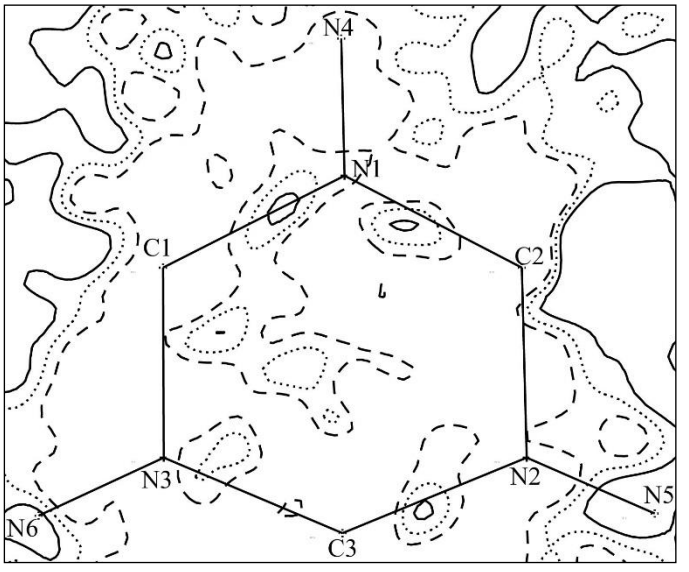

Figure 2. Residual density in the plane of the molecule. Solid lines shows positive contours, negative contours are dashed and zero contour are dotted. The contour interval is 0.05 eÅ-3

4.0 Structural Aspects

The ORTEP [21] plot of RDX molecule was depicted in Figure 3 showing the thermal ellipsoid atoms and the atom numbering scheme. The parallel bond distances in the six membered ring were almost equal with the maximum difference of 0.006(1) Å for C3–N3 [1.494(1) Å] and C2–N1[1.500(1) Å] bonds respectively. The trend was found to be similar in the reported[11] distances at room temperature, with the maximum difference of 0.008(4) Å for the same bonds. The C–N bond distances were ranges from 1.433(1) to 1.529(1) Å with the average distance 1.486(1) Å, which was 0.032 Å longer than that of reported C–N bonds. The N3–N6 bond distance [1.286(1) Å] was ~0.115(1) Å shorter than the other two parallel N–N bonds N2–N5 [1.419(1) Å] and N1–N4 [1.383(1) Å], while C.S. Choi et al reported that the decrement of N3–N6 bond distance from that of parallel N–N bonds by ~0.044 Å. This unique orientation of N3–N6 bond may be attributed from the effect of repulsive non-bonded interactions between adjacent nitro groups. The average N=O distance of unique nitrate group was ~1.284(1) Å, which was 0.070(1) Å longer than that of parallel nitrate groups [~1.214(1) Å], the similar trend appears in reported values. The average C–H bond distances from both low temperature and reported room temperature experiments were ~1.092(1) and ~1.080(8) Å respectively. On the whole it was found that the bond distances from the low temperature measurement were longer than that of reported room temperature measurement. The parallel nature of C1–N1 and C3–N2 bonds was reflected from the identical angles at N1 and N2 of the bonds C2–N1–C1 [113.2(3)°] and C2–N2–C3 [111.1(3)°]. The angles around N1 and N2 atoms in the outer ring bonds C1–N1–N4 [118.7(3)°], C2–N1–N4 [116.0(3)°], C3–N2–N5 [118.5(3)°] and C2–N2–N5 [117.8(3)°]

were found to be widen on compared with angles around N3, which makes N3–N6 bond flatter compared with other parallel N–N bonds. The angle at N6 atom [130.7(3)˚] in $-NO_2$ group was significantly larger than at N4 and N5 of other two $-NO_2$ groups and the angles were 126.6(4) and 124.0(4)˚ respectively. The six membered ring of RDX molecule was not planar, but adopts the chair confirmation which reveals from the gauche orientation of C1–N1 and C3–N2, bonds from the torsion angles -46.0(4)˚ [C2–N1–C1–N3] and 46.4(4)˚ [C2–N2–C3–N3] respectively. The atoms N1, C1, C3 and N2 form the base, and N3, C2 atoms lies 0.602(3) Å and -0.520(3) Å distance above and below of the base atoms. The three $N-NO_2$ groups inclined with the mean plane atoms at the angle of 50.9(2)˚ [$N1-NO_2$], 52.7(1)˚ [$N2-NO_2$] and 32.4(1)˚ [$N3-NO_2$] respectively.

The molecules in the unit cell were predominantly stabilized by C–H···O type of hydrogen bonding interaction. Figure 4 shows the dominant nature of O-atoms in the crystal packing having the density of 1.857 mg/m^3 calculated from cell parameter.

Table 1. Crystallographic Details

Crystal data	
Empirical formula	$C_3H_6N_6O_6$
Formula weight	222.14
Crystal system	Orthorhombic
Z, Space group	8, Pbca
a, b, c (Å)	10.587(3), 11.422(3), 13.138(4)
α (°), β (°), γ (°)	90.0
Multipole Refinement	
R(F)	0.032
wR(F²)	0.032
S	2.457
N_{ref}/N_v	26.61

5.0 Electron density

The topological analysis of the electron density has been performed for RDX molecule. The electron density of all the bonds with (3,-1) critical points which characterize the covalent bonds in RDX crystal were given in Table 2. The bond density $\rho_{bcp}(r)$ at C–N bonds in the six membered ring ranges from 1.62(3) to 1.86(1) eÅ^{-3}, with the maximum $\rho_{bcp}(r)$ of 1.86(1) and

1.85(1) eÅ^{-3} for the parallel bonds C1–N1 and C3–N2 respectively. This parallel heteronuclear bonds, which forms the mean plane, exhibits the maximum polarizability of about ~8.0% towards the carbon atoms due to the perturbations caused by other C–N bonds lies above and below mean plane atoms. The maximum deviation of BCP from the internulear axis was found for C2–N2 bond [0.042 Å] among the other bonds in the molecule. The N–N bonds appear to be of particular interest. All the N–N bonds in the RDX molecule were carrying markedly different densities, among these the N3–N6 bond density at bond critical point was 2.56(1) eÅ^{-3}, which was much higher than that of other N–N bonds, N1–N4 [2.22(1) eÅ^{-3}] and N2–N5 [2.07(1) eÅ^{-3}] respectively, however, the large electron density values ranges 1.98 to 2.31 eÅ^{-3} at bond critical point on N–N bonds was found for the explosive CL-20[10]. The electron density at the critical points on the N=O bonds were ranges 2.99 to 3.49 eÅ^{-3}, which were the highest electron density values in RDX molecule and thus was the best candidate for the bond to be considered as a double bond. The large charge accumulation was found for N5–O3 [3.46(3) eÅ^{-3}] and N5–O4 [3.49(1) eÅ^{-3}] on compare with other two nitro groups N4–O1 [3.44(3) eÅ^{-3}], N4–O2 [3.39(1) eÅ^{-3}] and N6–O5 [3.03(3) eÅ^{-3}], N6–O6 [2.99(1) eÅ^{-3}] respectively. The high electron density values on the N=O bonds except N6=O5, can be effect of electron donation from oxygen lone pairs, since they are not involved in hydrogen bonding in the crystal. The polarization of N–N [~2.2%] and N=O [~3.6%] bonds were relatively smaller than C–N bonds of the RDX molecule. Figure 5(a-c) shows the deformation density of N–NO_2 groups in the RDX molecule. The average electron density in C–H bond regions of the six membered ring was ~1.83 eÅ^{-3}, with the polarity values close to 17.5% towards hydrogen.

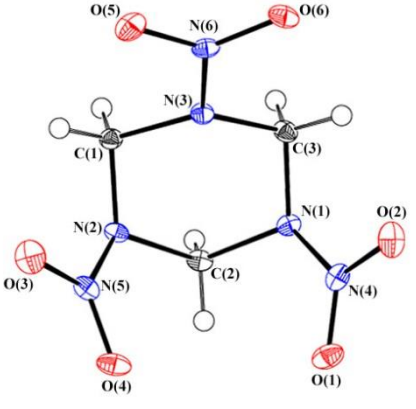

Figure 3. Molecular structure of RDX Figure 3. Molecular structure of RDX

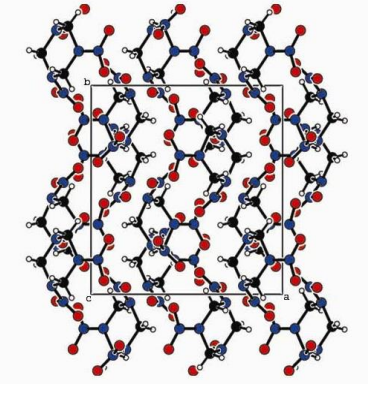

Figure 4. Molecular packing in the crystal

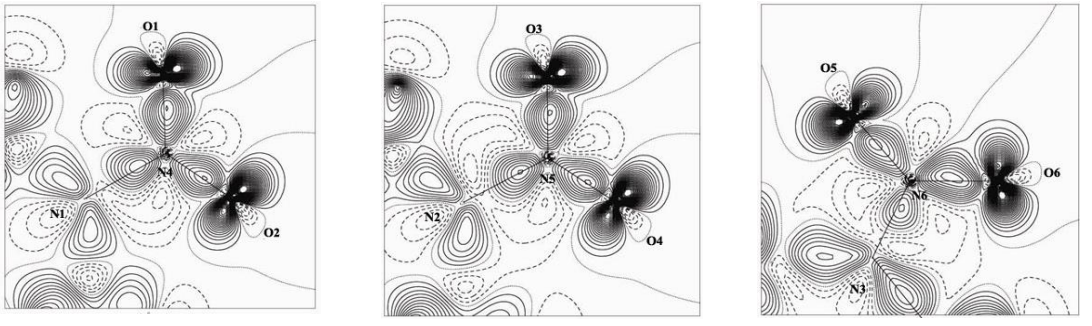

Figure 5(a-c). Deformation density maps of N–NO_2 groups of the molecule. Sold lines positive contours; dashed lines negative contours and dotted lines zero contours. Contour intervals at 0.05 eÅ^{-3}.

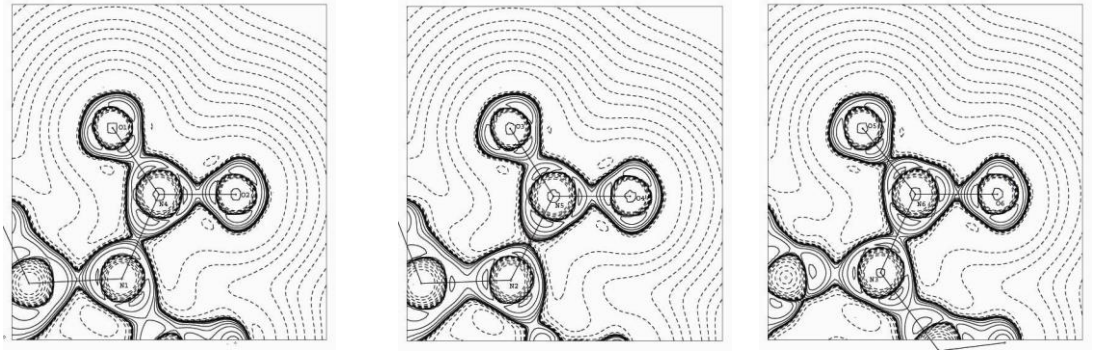

Figure 6(a-c). Laplacian of electron density of N–NO_2 groups of the molecule. Solid lines positive contours; dashed lines are negative contours. Contours are drawn on a logarithmic scale, 3.0 x 2^N eÅ^{-5}.

6.0 Bond Topological Analysis

Bond topological analysis [22] was clearly predicted from Laplacian of charge distribution $\nabla^2\rho_{bcp}(r)$ at the bond critical points. As expected, the parallel bonds C1–N1 and C3–N2, having high electron density values, exhibit the most negative Laplacian -16.3(1) and -16.1(1) eÅ^{-5} attributes the maximum depletion of charges among the C–N bonds of the molecule at the bond critical points. The Laplacian of electron density in the plane of three nitro groups were shown in figure 6(a-c). The solid contours show the negative value of the laplacian i.e. they represent the accumulation of electron density in the crystal. For the RDX molecule, this accumulation was mostly around the atoms and along the chemical bonds. For the oxygen atoms, the electron density concentrates mainly in the non-bonding directions, which emphasize the lone pair region. The $\nabla^2\rho_{bcp}(r)$ values for N=O bonds ranges -5.5(1) eÅ^{-5} to -14.9(1) eÅ^{-5}. Notably,

the N6–O5 and N6–O6 bonds possess maximum electron density, has less Laplacian of -5.5(1) and -7.4(1) eÅ^{-5} at its critical points on compare with other N–O bonds. The topological analysis in p-nitroaniline [23], lithium bis(tetramethylammonium) hexanitro-cobaltate(III) [24] and trans-tetra-aminedinitronickel(II) [25] also shows high electron density values at the critical points in the N–O bonds of 3.19 to 3.61 eÅ^{-3} and small absolute values of the Laplacian of -3.4 to -11.9 eÅ^{-5}. Analysis of bond topological properties of N–N bonds was found to be of significant chemical interest. Though the electron density values at the critical points on N–N bonds were relatively high on compare with other bonds except N=O bonds, the absolute values of the Laplacian are less on compared with other bonds in the RDX molecule and the values are -1.8(1) [N1–N4], -0.4(1) [N2–N5] and -4.4(1) eÅ^{-5} [N3–N6] respectively. The topological analysis in CL-20, also shows high electron density values at the critical points in the N–N bonds of 1.98(1) to 2.31(1) eÅ^{-3} and small absolute value of Laplacian of 1.8(1) to -6.1(1) eÅ^{-5}. This was due to the high positive value for λ_3 eigen value for N1–N4 [31.4 eÅ^{-5}], N2–N5 [30.1 eÅ^{-5}] and N3–N6 [34.4 eÅ^{-5}], indicating that the charge depletion in the bond direction was significantly higher than that of the other bonds. The same feature was also observed in trinitrodiazapentalene (TNDP) [9]. As per above results, it was found that the N–N bonds should be weak, in particular N1–N4 and N2–N5 be the first to break during the chemical decomposition. The ellipticities were smaller for the ring bonds C–N [~0.09] than for N–N [~0.23] and N=O [~0.12] bonds. These values were similar to those observed in CL-20.

7.0 Atomic Charges and Electrostatic Potential

The atomic charges were calculated from the monopole population (P_v) of the final refinement, (i.e) q = N - P_v, where N is the number of valence electrons for the neutral atoms [26]. Further, the AIM charges [27,28] were also calculated for all atoms from the charge integration of electron density distribution (EDD) within the atomic basin using TOPXD [23] routine incorporated to XD program. These results were summarized in Table 3. Both the definition agrees on the broad picture of positive nitrogen and negative oxygen atoms of nitrate groups, though the actual values vary significantly within this. The monopole charges of the carbon atoms in the six membered ring are highly negative [-0.27(1) e], reflecting the fact that it attracts the large amount of electron density from its two hydrogen atoms. However, the CH_2 moiety remains positive when the hydrogen atomic charges are included [CH_2: +0.15 e]. On the other hand, the AIM charges of the carbon atoms are highly positive [+0.24 e], due to electronegative nitrogen atoms [-0.50 e] bonded to these carbon atoms, though have almost equal actual values as their monopole charges. The monopole charges for –NO_2 fragments attached at N1, N2 and N3 atoms, having the monopole charges of 0.07(1) e, are -0.22(1) e which attributes the hyperconjugation effect and make the N–NO_2 bonds be highly polarized. This confirms the weakness of N–N bonds in the RDX molecule. The monopole and AIM charges of H-atoms were nearly equal and they were closed to 0.20 e.

Table 2. Topological properties at the BCP

Bond	ρ(eÅ-3)	2 ρ (eÅ-5)	E	D1 (Å)	d2 (Å)	D(Å)	Δd%	r (Å)
N1–C1	1.86(1)	-16.3(1)	0.12	0.832	0.602	1.434	8.0(C1)	0.009
N1–C2	1.62(3)	-8.5(1)	0.07	0.840	0.662	1.502	5.9(C2)	0.020
N2–C2	1.65(1)	-9.0(1)	0.05	0.838	0.696	1.533	4.6(C2)	0.042
N2–C3	1.85(1)	-16.1(1)	0.10	0.831	0.604	1.435	7.9(C3)	0.013
N3–C3	1.77(1)	-12.2(1)	0.08	0.824	0.671	1.495	5.1(C3)	0.022
N3–C1	1.64(1)	-8.4(1)	0.13	0.836	0.697	1.533	4.5(C1)	0.037
N1–N4	2.22(1)	-1.8(1)	0.22	0.660	0.724	1.384	2.3(N1)	0.022
N2–N5	2.07(1)	-0.4(1)	0.25	0.675	0.743	1.418	2.4(N2)	0.007
N3–N6	2.56(1)	-4.4(1)	0.21	0.618	0.668	1.286	1.9(N3)	0.016
N4–O1	3.44(3)	-14.6(1)	0.13	0.547	0.664	1.211	4.8(N4)	0.002
N4–O2	3.39(1)	-14.9(1)	0.10	0.559	0.669	1.227	4.5(N4)	0.014
N5–O3	3.46(3)	-15.2(1)	0.13	0.545	0.662	1.207	4.8(N5)	0.002
N5–O4	3.49(1)	-17.2(1)	0.09	0.549	0.664	1.214	4.7(N5)	0.009
N6–O5	3.03(3)	-7.4(1)	0.10	0.606	0.687	1.292	3.1(N6)	0.022
N6–O6	2.99(1)	-5.5(1)	0.14	0.592	0.686	1.279	3.7(N6)	0.002
C1–H1	1.83(1)	-17.2(1)	0.07	0.739	0.354	1.092	17.6(H1)	0.006
C1–H2	1.84(1)	-18.2(1)	0.08	0.738	0.356	1.094	17.5(H2)	0.016
C2–H3	1.84(1)	-18.1(1)	0.07	0.737	0.357	1.094	17.4(H3)	0.016
C2–H4	1.82(1)	-17.2(1)	0.07	0.737	0.355	1.093	17.5(H4)	0.008
C3–H5	1.82(1)	-17.3(1)	0.07	0.738	0.354	1.092	17.6(H5)	0.010
C3–H6	1.84(1)	-18.1(1)	0.07	0.739	0.356	1.095	17.5(H6)	0.016

The molecular electrostatic potential (MEP) was calculated from the multipole refinement, having the ability to derive MEP for the isolated molecule in the crystalline environment. Further it also helps to evaluate the Murray et al's [29] hypothesis that a key factor in determining the impact sensitivity of the compound may be extent to which the stabilizing the effect of charge delocalization has been concentrated. The calculated MEP, according to the method by su and coppens [30], were visualized in XDGRAPH and displayed in figure 7(a). As expected, the negative regions (red) around oxygen atoms of the three nitro groups and positive (blue) resides on the rest of the molecule were observed. These potentials represent the sites of electrophilic and electrophobic attacks. The shape of the electronegative surface over the oxygen atoms was interesting, as it shows the slight difference between O(5), which is involved in intermolecular hydrogen bond, and remaining oxygen atoms. The hydrogen bond interaction deconvolutes the electronegative character of O(5) and preventing it from attracting the external positive charge. Since the nitro groups and CH_2 groups pointing in the opposite directions, the either side of the ring exhibit complementary electrostatic potential regions. This was in accord

with the large molecular dipole moment 6.8(2) Debye, which indicates the large separation of positive and negative charges. The polarization of N–NO_2 bonds was clearly exhibited from positive and negative potential around N and –NO_2 regions, which again reveals the weakness of N–N bonds. The shape of ESP between two symmetrically sitting molecules in the crystal field environment was shown in the figure 7(b).

Table 3. Atomic charges (e)

Atom	q(P$_v$)	q(Ω)
C1	-0.27(1)	0.24
C2	-0.27(1)	0.22
C3	-0.27(1)	0.25
N1	0.07(1)	-0.53
N2	0.07(1)	-0.51
N3	0.07(1)	-0.47
N4	0.16(1)	0.76
N5	0.16(1)	0.77
N6	0.16(1)	0.68
O1	-0.19(1)	-0.45
O2	-0.19(1)	-0.45
O3	-0.19(1)	-0.44
O4	-0.19(1)	-0.46
O5	-0.19(1)	-0.41
O6	-0.19(1)	-0.40
H1	0.21(1)	0.2
H2	0.21(1)	0.19
H3	0.21(1)	0.19
H4	0.21(1)	0.21
H5	0.21(1)	0.21
H6	0.21(1)	0.19

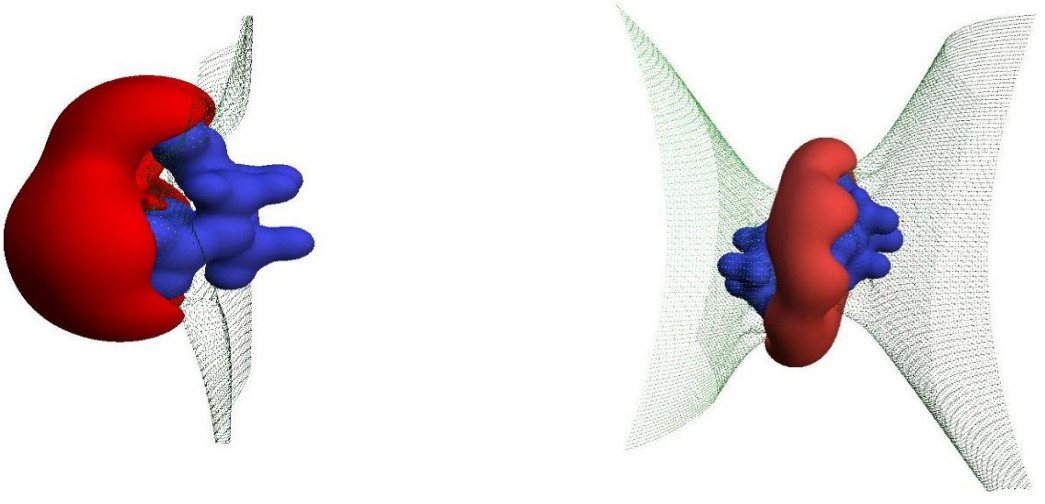

Figure 7. Isosurface representation of Electrostatic potential of (a) isolated molecule and (b) symmetrically sitting two molecules in the crystal. Blue (+0.5 eÅ^{-1}) and red (-0.2 eÅ^{-1}) regions are positive and negative ESP respectively. Grey grid indicate the zero ESP.

8. Conclusion

The geometrical and bond topological properties of RDX molecule were determined from low temperature X-ray diffraction data. The significant differences were observed in bond distances when compared with that obtained from reported room temperature measurement. The bond topological analysis has been carried out from multipole refinement. From the position of the critical points, significant polarization of C–N and C–H bonds may be concluded, however the N–O and N–N bonds were less polarized. The present results obtained from bond topological analysis reveals the strength of the entire bonds in the molecule. Among all other bonds in the RDX molecule, the N–N bonds were found to be weak, which was predicted from small negative Laplacian values. Specifically, N3–N6 bonds, having shorter bond length, has large charge accumulation and concentrated charges [-4.4(1) eÅ^{-5}] at the bond critical point. On the other hand, the longer N1–N4 and N2–N5 bonds has low electron density and the charges were depleted, as their $\nabla^2\rho_{bcp}(r)$ values were -1.8(1) and -0.4(1) eÅ^{-5} respectively. Based on these results, it was cleared that the bond properties of N–N bonds strongly depends upon the equilibrium bond length. It is concluded from the above results, on decomposition, the N–N bonds were expected to break first. The molecular electrostatic potential of the RDX molecule clearly indicates the possible reactive surface in the molecule from electro positive and electro negative regions. In particular, the high negative electro potential resides on one face of the molecule and

electro positive potential on the other side, which attributes high performance character of the RDX molecule.

References

[1] G. I. Brown, (1998) The Big Bang, A History of Explosives, *Sutton Publishing*, UK.

[2] I. Khan, Coming of Gunpowder to the Islamic World and North India, Spotlight on the Role of the Mongols, *J. Asian Hist.,* 30 (1996) 41–50.

[3] I. Khan, (1996) The Role of the Mongols in the Introduction of Gunpowder and Firearms in South Asia, In Buchanan, Brenda J. *Gunpowder, The History of an International Technology*, *Bath University Press*, Bath.

[4] I. Khan, (2004) Gunpowder and Firearms, Warfare in Medieval India, *Oxford University Press*, Oxford, UK.

[5] P. Politzer, J.S. Murray, (Eds) Energetic Materials, *Theoretical and Computational Chemistry Series*, *Elsevier*, New York, 12 (2003).

[6] E. A. Zhurova, A. A. Pinkerton, Chemical bonding in energetic materials: [beta]-NTO, *Acta Cryst. B*, B57 (2001) 359–365.

[7] E. A.Zhurova, V. G. Tsirelson, A. I.Stash, M. V. Yakovlev, A. A.Pinkerton, Electronic Energy Distributions in Energetic Materials: NTO and the Biguanidinium Dinitramides, *J. Phys. Chem. B*, 108 (2004) 20173–20179.

[8] E. A. Zhurova, A. I.Stash, V. V. Z.Mikhail, E. V. Barthashevich, V. A. Potemkin, & A. A. Pinkerton, Atoms-in-Molecules Study of Intra- and Intermolecular Bonding in the Pentaerythritol Tetranitrate Crystal, *J. Am. Chem. Soc.*, 128 (2006)14728–14734.

[9] Y.-S.Chen, , A. I. Stash& , A. A Pinkerton, Chemical bonding and intermolecular interactions in energetic materials: 1,3,4-tri-nitro-7,8-di-aza-pentalene, *ACTA CRYSTALLOGR B,* B63(2007) 309-318.

[10] A. Meents, B. Dittrich, S.K.J.Johnas, V. Thome, & E.F. Weckert, Charge-density studies of energetic materials: CL-20 and FOX-7. Corrigendum, *ACTA CRYSTALLOGR B*, B64 (2008) 42-49.

[11] C.S. Choi, E. Prince, The crystal structure of cyclotrimethylenetrinitramine, *ACTA CRYSTALLOGR B*, B28 (1972) 2857-2862.

[12] N.K. Hansen, P. Coppens, Testing aspherical atom refinements on small-molecule data sets, *Acta Cryst. A*, 34 (1978) 909-921.

[13] R. F. W.Bader, H. J.Essen, Bonded and nonbonded charge concentrations and their relation to molecular geometry and reactivity, *J. Am. Chem. Soc.*, 106 (1984) 1594-1605.

[14] Bruker, *APEX*. Bruker AXS Inc, Madison, Wisconsin, USA, (2000).

[15] Bruker, *SAINT*, Bruker AXS Inc, Madison, Wisconsin, USA, (2000).

[16] G.M. Sheldrick, (1998) *SHELXS97*, Programs for Crystal Structure Analysis (Release 97-2), Institut fur Anorganische Chemie der Universitat, D-3400 Gottingen, Germany.

[17] G.M. Sheldrick, (1998) *SHELXL97*, Programs for Crystal Structure Refinement (Release 97-2), Institut fur Anorganische Chemie der Universitat: D-3400 Gottingen, Germany.

[18] T. Koritsanszky, P. Macchi, C. Gatti, L.J. Farrugia, P. R. Mallinson, A. Volkov, T. Richter, *XD-2006*, A Computer Program Package for Multipole Refinement and Topological Analysis of Charge Densities and Evaluation of Intermolecular Energies from Experimental or Theoretical Structure Factors, Version 5.33, (2007).

[19] H.Frank Allen, Olga kennard, G. David, Watson, Lee Brammer, A. Guy orpen, Robin Taylor. Tables of Bond length determined by X-Ray and Neutron Diffraction. Part 1 Bond lengths in organic compounds, *J. Chem. Soc, Perkin Transactions,* (1987).

[20] V. Anatoliy, Y.A. Abramov, & P. Coppens, Aspherical-atom scattering factors from molecular wave functions. 1. Transferability and conformation dependence of atomic electron densities of peptides within the multipole formalism, *Acta Cryst. A,* A58 (2000) 406-472.

[21] L. J. Farrugia, ORTEP-3 for Windows - a version of ORTEP-III with a Graphical User Interface (GUI), *J. Appl. Crystallogr*, 30 (1997) 565.

[22] R.F.W. Bader, (1990) Atoms in Molecules- A Quantum Theory, *Clarendon press*, oxford.

[23] A.Volkov, C. Gatti, Y. A. Abramov, P.Coppens, Evaluation of net atomic charges and atomic and molecular electrostatic moments through topological analysis of the experimental charge density, *Acta Cryst. A,* 56 (2000) 252-258.

[24] R. Bianchi, C. Gatti, V. Adovasio, M. Nardelli, Theoretical and experimental (113 K) electron-density study of lithium bis(tetramethylammonium) hexanitrocobaltate(III), *Acta Cryst. B*, 52 (1996) 471-478.

[25] B.B. Iversen, F.K. Larsen, B.N. Figgs, P.A. Reynolds, X-Ray–neutron diffraction study of the electron-density distribution in trans-tetraaminedinitronickel(II) at 9 K: transition-metal bonding and topological analysis, *J. Chem. Soc., Dalton Transactions,* (1997) 2227-2240.

[26] P. Coppen, (1997) X-ray Charge density and Chemical bonding, *Oxford Science Publications*, Oxford, UK.

[27] F. W.Biegler-Konig, R. F. W. Bader, T.Ting-Hau, Calculation of the average properties of atoms in molecules. II, *J. Comput. Chem.*, 3 (1982) 317-328.

[28] R.F. W.Bader, T.T. Nguyen-Dang, Quantum Theory of Atoms in Molecules–Dalton Revisited, *Adv. Quantum. Chem.*14 (1981) 63-124.

[29] J.S. Murray, P. Lane, & P. Politzer, Relationships between impact sensitivities and molecular surface electrostatic potentials of nitroaromatic and nitroheterocyclic molecules, *Mol. Phys,* 85 (1995) 1-8.

[30] Z.Su, P. Coppens, On the mapping of electrostatic properties from the multipole description of the charge density, *Acta Cryst. A*, A48 (1992) 188-197.

Acknowledgements: NIL

Conflict of interest: NIL